Available online at www.CivileJournal.org

Civil Engineering Journal

(E-ISSN: 2476-3055; ISSN: 2676-6957)

Vol. 9, No. 07, July, 2023

Experimental and Analytical Study on Postfire Reinforced Concrete Beams Retrofitted with CFRP in Flexure and Shear

Vu Nguyen Nguyen [1, 2], Vui Van Cao [1, 2*]

[1] *Faculty of Civil Engineering, Ho Chi Minh City University of Technology (HCMUT), District 10, Ho Chi Minh City, Vietnam.*

[2] *Vietnam National University Ho Chi Minh City, Linh Trung Ward, Thu Duc City, Ho Chi Minh City, Vietnam.*

Received 10 March 2023; Revised 11 June 2023; Accepted 18 June 2023; Published 01 July 2023

Abstract

In this study, experiments were performed on carbon fiber reinforced polymer (CFRP) retrofitted postfire reinforced concrete (RC) beams, followed by theoretical analyzes. Experiments were conducted on eleven RC beams, which were exposed to different fire durations and retrofitted with CFRP in flexure and shear. The experimental results indicated that fire shifted the flexure failure to the flexure-shear failure of postfire RC beams. CFRP retrofitted postfire RC beams experienced progressive peeling-off failure. FRP retrofitting significantly increased the yield deflection by 58.2−97.3% but decreased the ultimate deflection by 43.0−55.5% compared with that of the control beam. Consequently, the ductility was reduced by 69.7−74.7%, categorized as low ductility. CFRP retrofitting successfully increased the strengths of 30-min postfire beams by up to 23.1% higher than those of the control beam. Fire significantly decreased the stiffness of postfire beams by 46.4−49.2% compared with that of the control beam, whereas CFRP retrofitting did not fully recover the stiffness of postfire beams. Finally, a simple model of the moment capacity of postfire beams without/with CFRP retrofits was developed based on the practicability of limited data feasibly obtained from real fires. The proposed model, with its simplicity, practicability, and reasonable accuracy, can be a useful tool for structural engineers in the FRP retrofitting of postfire RC structures.

Keywords: Fire; CFRP; Retrofitting; Reinforced Concrete; Beam.

1. Introduction

Fire negatively affects structures and results in various damage extents, including collapse [1, 2]; therefore, postfire members/structures cannot perform their original design function. Except in cases of collapse [3, 4], post-fire buildings fall somewhere between the two options: 1) demolishing and rebuilding or 2) retrofitting. The second option seems preferable since it is significantly more cost-effective than the first one. To meet the requirements of the original design, postfire structures must be retrofitted to improve their performance.

Fiber-reinforced polymer (FRP) has demonstrated itself as a material of choice for retrofitting buildings in general and post-fire buildings because of its flexible and favorable properties, e.g., high strength, high corrosion resistance, low weight, ease of usage, and quick construction. FRP applications for reinforcement of structures have drawn a lot of attention from academics worldwide in recent decades [5, 6]. Researchers' findings were incorporated into retrofitting design guidelines such as ACI 440.2R-17 [7]. FRP can be used to wrap concrete columns to increase their axial load-carrying capacity [8–10]. FRP can also be used for shear strengthening [11–13] and flexural strengthening [14, 15]. With its flexible characteristics, FRP can be used for combined retrofitting [16]. FRP can be used to repair damaged

* Corresponding author: cvvui@hcmut.edu.vn

http://dx.doi.org/10.28991/CEJ-2023-09-07-05

© 2023 by the authors. Licensee C.E.J, Tehran, Iran. This article is an open access article distributed under the terms and conditions of the Creative Commons Attribution (CC-BY) license (http://creativecommons.org/licenses/by/4.0/).

reinforced concrete (RC) structures [17–19], or damaged concrete [20]. FRP offers various solutions using the externally bonded (EB) technique [21] and near-surface mounted (NSM) technique [22–24]. External bonded reinforcement on grooves (EBROG) is another solution [25], which was reviewed by Sanginabadi et al. [26]. Such FRP solutions are almost free from problems of modifying the architecture, occupying the living space of buildings, or adding load to structures when compared with conventional retrofitting methods, e.g., steel braces or sectional enlargement.

The EB technique is commonly used for FRP retrofitting, and its effectiveness has been confirmed by researchers. Sharif et al. [21] conducted experiments on the efficacy of EB FRP strengthening of preloaded RC beams and discovered that the increase in FRP thickness increased the flexural strength but reduced the ductility. EB carbon fiber reinforced polymer (CFRP) retrofitting significantly increased the ultimate load-carrying capacity of pre-cracked RC beams [27]. Spadea et al. [28] found that EB CFRP considerably reduced the ductility and deformation capacities of RC beams, whereas adequate anchorages increased the ductility and load-carrying capacity by about 65% and 70%, respectively. EB FRP retrofitting increased the flexural strength of pre-cracked RC beams while the failure became more brittle [29]. EB CFRP can be used to repair corroded RC beams [30], and EB FRP retrofit recovered the corroded RC beams to the control RC beams [31]. EB FRP retrofitting significantly increased the ultimate deformation capacity [32]. The ultimate load-carrying capacity of EB FRP retrofitted RC beams was 230% of the control beam [33]. White et al. [34] examined the response of RC beams retrofitted with EB CFRP laminates under various loading rates and discovered that the loading rates did not affect the ductility and failure mechanism. In addition, EB CFRP strengthening decreased ductility and energy absorption but increased flexural strength and stiffness. Malek & Patel [35] derived equations for designing RC beams that were strengthened with EB FRP laminates. The damaged RC beams retrofitted with EB CFRP laminates had much higher stiffness and load-carrying capacity than the control beam [36]. Jeevan and Jagannatha Reddy [37] found that EB CFRP strengthening without/with anchorages increased the load-carrying capacity of CFRP retrofitted RC beams by 34.0% and 48.5% compared with that of the control beam, respectively. Recently, Al-Ghrery et al. [38] found that EB CFRP increased the flexural load-carrying capacity, and the retrofitted RC beams failed by intermediate cracked debonding. Choi et al. [39] evaluated the long-term behavior of 15-year-old RC beams retrofitted with EB glass FRP (GFRP) and confirmed the long-term effectiveness of this retrofitting. Li et al. [40] developed a model to predict the flexural strength of RC beams retrofitted with CFRP, considering the intermediate crack. EB FRP strengthening investigations have been thoroughly reviewed by Fayyadh & Razak [41] and most recently by Askar et al. [42].

In narrowing the discussion on FRP retrofitting of postfire RC beams, different aspects have been investigated by researchers. Liu et al. [43] analyzed failure modes of CFRP retrofitted RC beams exposed to fire and showed that fire significantly decreased the shear capacity, leading to shear failure of retrofitted beams in fire. The fire behavior of RC beams was not always improved by increasing the fire insulation thickness. Ahmed & Kodur [44] tested one control RC beam and four EB CFRP retrofitted RC beams simultaneously subjected to load and fire and found that the anchorage configurations had a substantial impact on the deflection of the retrofitted beams. RC beams, which were strengthened with FRP and had a 25-mm-thick insulating layer, were able to endure the test fire. Yu and Kodur [45] tested four RC T-sectional beams retrofitted with near-surface mounted (NSM) FRP under load and fire with consideration of fire protection. The results indicated that, under sustained service loads, NSM FRP retrofitted RC T beams without fire protection could have a fire resistance of up to 3 h. NSM FRP retrofitted RC T beams under higher service loading can achieve a similar fire resistance to the control beam. NSM FRP could resist the tensile forces if its anchorage zone was well protected. Jiangtao et al. [46] indicated that the fire resistance of NSM CFRP retrofitted RC beams could be more than 3 h if appropriate fire protection was used. Their experimental results also proved that NSM CFRP strengthening exhibited much better fire performance than EB CFRP strengthening. Truong et al. [47] found that GFRP strips using epoxy beneficially retained the flexural strength of retrofitted postheated RC beams. However, the effect of GFRP strips using mortar on deformability was more pronounced than that on flexural strength. Recently, Nguyen & Van Cao [48] confirmed that NSM GFRP retrofitting recovered and increased the strength of postfire RC beams by 39% compared with control RC beams. Fire and NSM GFRP significantly changed the flexure failure to peeling-off failure of concrete between GFRP and steel, decreasing the ductility. NSM GFRP slightly improved the elastic stiffness and significantly increased the plastic stiffness.

FRP retrofitting has been extensively investigated for RC structures at normal temperature conditions; however, it seems to be less explored for those after fire exposure. In addition, postfire structures experienced reductions in both flexural and shear capacities. Thus, these structures need to be retrofitted in flexure and shear, which seem to have been limitedly investigated as reviewed above. In this direction, this study aimed at combining flexural and shear EB CFRP to strengthen postfire RC beams. To achieve this aim, experiments on eleven RC beams were performed, followed by analytical investigations. In the experiments, ten RC beams were exposed to fire and then retrofitted with both flexural and shear CFRP using different numbers of U wraps. These ten retrofitted postfire beams and the control beam were loaded until failure. The test results were analyzed and discussed to come up with conclusions. In theoretical analyzes, the load-carrying capacities of postfire RC beams without/with FRP retrofitting were calculated and compared with those obtained from the experiments. The comparisons indicated a reasonable agreement between the two results. A model was proposed to predict the load-carrying capacity of CFRP-retrofitted postfire RC beams, which can be a helpful tool for engineers in practice.

2. Experimental Program

2.1. Materials and RC Beams

The mix per m^3 of concrete included 327 kg of PC 40 cement, 0.880 m^3 of stone aggregate (coarse aggregate) with a maximum size of 22 mm, 0.475 m^3 of river sand (fine aggregate) with a maximum size of 4 mm, and 185 L of water. Three cylinder samples of concrete with a diameter × height = 150×300 mm were taken. Their average compressive strength at 28 days was 24.3 MPa. The length and cross section of the tested beams were 1800 mm and 150×200 mm, respectively. The longitudinal steel was 4ϕ14 and the transverse steel was ϕ6 with intervals of 100 mm. Six ϕ14 steel samples had an average yield and ultimate stresses of 443.6 MPa and 535.4 MPa, respectively. Six ϕ6 steel samples had an average yield and ultimate stresses of 334.9 MPa and 466.4 MPa, respectively. The steel arrangement and dimensions of the tested beams are shown in Figure 1. The concrete cover had a thickness of 25 mm, which was measured at the center of the ϕ6 stirrups. CFRP was used for retrofitting postfire RC beams. A CFRP layer had a thickness of 0.131 mm. The average tensile strength of six CFRP specimens was 2825.6 MPa.

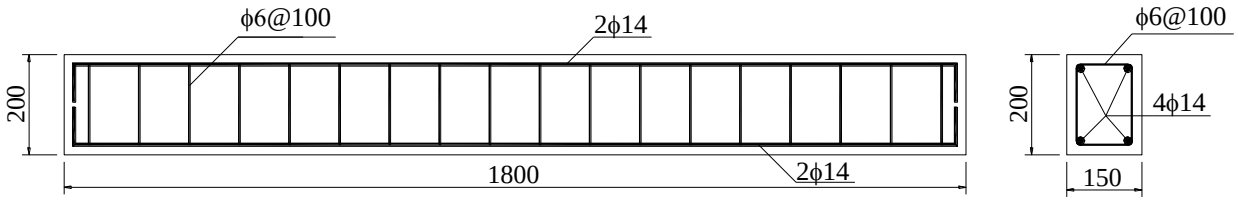

Figure 1. Dimensions and steel arrangement (in millimeter)

Figure 2-a shows the steel reinforcement and formwork of eleven tested beams prior to concrete casting. Figures 2-b and 2-c show these RC beams after casting concrete and after removing the formwork, respectively. The flowchart of the experiments is shown in Figure 2-d. The labels of these beams were permanently written at the beam ends, and printed labels were temporarily attached for picture-taking purposes. The structure of beam labels is "Bt-Ui", where B designates the beam, t is the fire exposure duration of 30 and 60 min, U designates the U-wrapping, and i = 1, 2, 3, and 4 are the number of U-CFRP pairs wrapped at each beam end. For example, B30-U2 means that this RC beam was exposed to a 30-min fire and was then retrofitted with CFRP configuration U2. Table 1 shows details of the tested RC beams, including names, fire durations, and CFRP retrofitting. These beams were classified into three groups by fire duration, namely B0, B30, and B60. Group B0 included one beam B0. Group B30 included one beam B30 and four CFRP retrofitted postfire beams. Group B60 was similar to group B30 but the fire duration was 60 min. Beam B0 is the control beam, while beams B30 and B60 can also be considered the control beams of groups B30 and B60, respectively. Four retrofitting configurations, namely U1, U2, U3, and U4, are presented in Section 2.3. For convenience, four retrofitted postfire beams of groups B30 and B60 can be sub-grouped as B30-U and B60-U, respectively.

a) Reinforcement and formwork

b) Beams after casting and concrete samples

c) RC beams

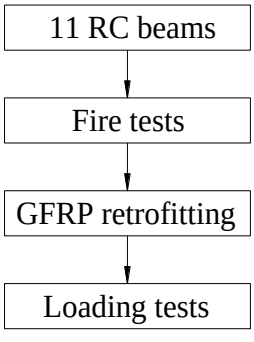

d) Flowchart of the experiments

Figure 2. Reinforcement, concrete casting, RC beams, and the flowchart

Table 1. Labels and retrofitting of beams

No.	Group	Beam name	Fire duration (min)	FRP retrofitting
1	B0	B0	0	No
2	B30	B30	30	No
3		B30-U1	30	FRP retrofitting U1
4		B30-U2	30	FRP retrofitting U2
5		B30-U3	30	FRP retrofitting U3
6		B30-U4	30	FRP retrofitting U4
7	B60	B60	60	No
8		B60-U1	60	FRP retrofitting U1
9		B60-U2	60	FRP retrofitting U2
10		B60-U3	60	FRP retrofitting U3
11		B60-U4	60	FRP retrofitting U4

2.2. Fire Tests

RC beams of groups B30 and B60 were subjected to fire for 30 and 60 min, respectively. Figure 3-a shows an RC beam installed in the furnace. The primary components included an oil burner and a 1200ºC-capacity thermocouple system. The secondary components included a steel frame structure, layers of high-temperature-resistant bricks, two cover blocks, and an exhausted pipe. A manual adjustment button on the oil burner was used to control the oil volume injected for burning, allowing the temperature to closely follow the desired temperature curve during the tests. It is easier to spot flames at night time than at day time; thus, night time is safer to control fire. Night time was therefore chosen to conduct fire tests due to safety concerns. Throughout the fire tests, including the cooling phase, the temperature in the furnace was measured and recorded every 15 seconds. Figure 3-b shows an RC beam in the furnace after a fire test, while Figure 3-a shows that beam before the fire test. It is evident that the surface of the concrete changed from grey colour of normal concrete to pale pink. Figure 3-c shows ten RC beams after the fire tests in comparison with the control beam B0 (without fire exposure). The surfaces of postfire beams appeared to have hair cracks with different lengths. Some local minor spalling of concrete was also observed.

a) A beam in the furnace before fire test

b) A beam in the furnace after fire test

c) RC beams after fire tests

Figure 3. Fire test setup

Figures 4-a and 4-b plot the obtained temperature–time curves of group B30 and B60 beams, respectively. For comparison, the ISO 834 temperature–time curve is also plotted. Overall, because the oil intake was manually adjusted throughout the tests, the measured curves closely followed the ISO 834 curve. The temperature is slightly higher than the ISO 834 curve.

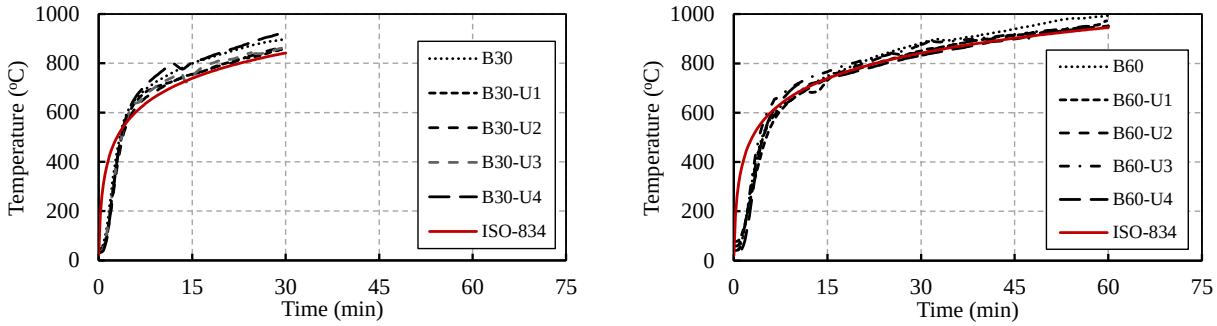

a) Group B30 beams b) Group B60 beams

Figure 4. Temperature–time curves

2.3. FRP Retrofitting

After fire exposure and cooling down to ambient temperature of ten RC beams, of each postfire group, one beam was not retrofitted, while the remaining four beams were retrofitted with four CFRP retrofitting configurations U1–U4, as shown in Figures 5-a to 5-d. Figures 5-e and 5-f show cross sections A-A and B-B of CFRP retrofitted RC beams at the locations without and with U-wraps, respectively. The flexural CFRP included two 200-mm-width CFRP layers that were longitudinally bonded on the bottom surface and extended 25 mm on the two side surfaces. The length of flexural CFRP is 1600 mm. After two layers of flexural CFRP were bonded, CFRP U-wraps were applied. CFRP U-wraps included 1, 2, 3, and 4 pairs at each beam end, namely U1–U4, respectively. For example, U3 means three pairs of U wraps at each beam end. Figure 5-g shows eleven beams after retrofitting to be ready for the loading tests. In Figure 5-g, the farthest beam is the control beam B0; five beams on the left are of group B30; and five beams on the right are of group B60.

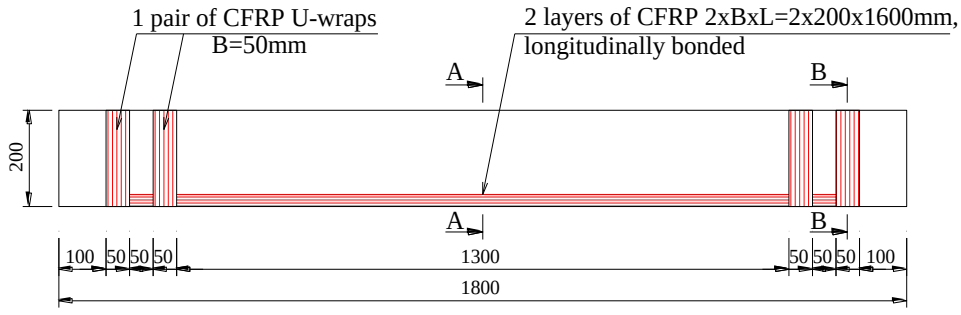

a) FRP retrofitting U1

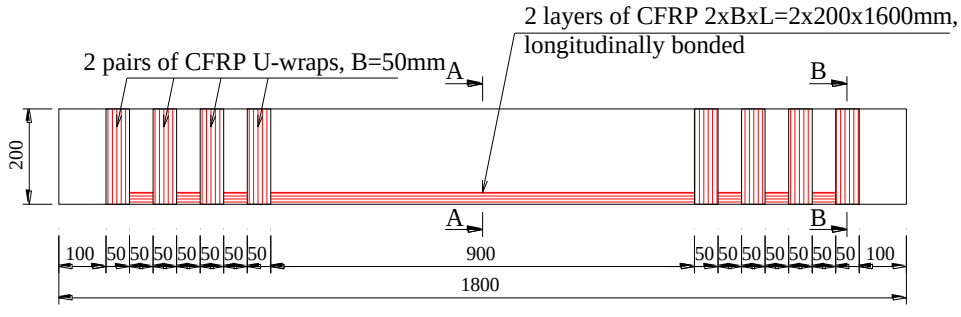

b) FRP retrofitting U2

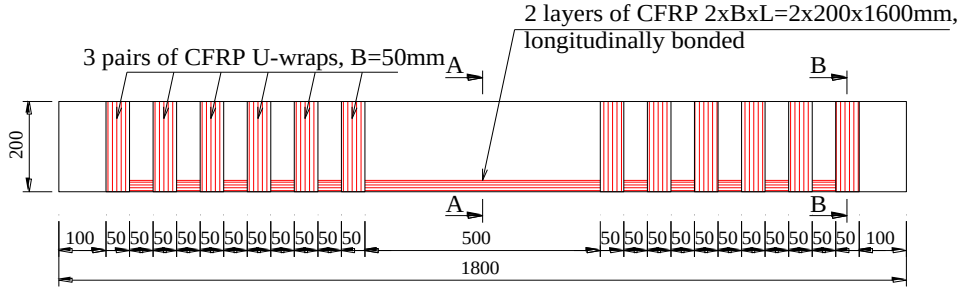

c) FRP retrofitting U3

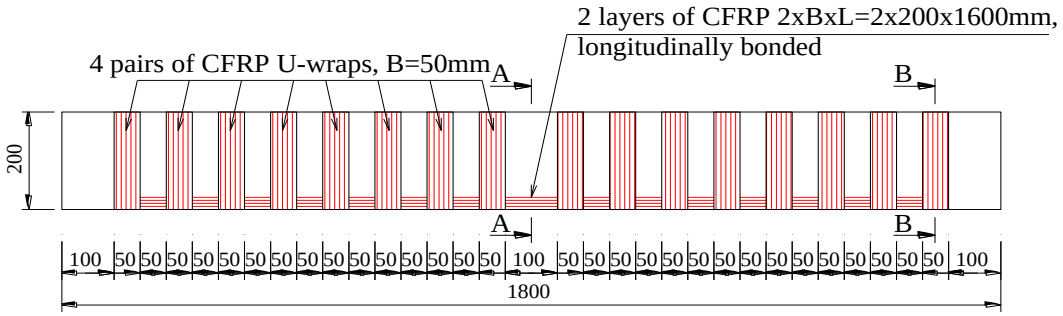

d) FRP retrofitting U4

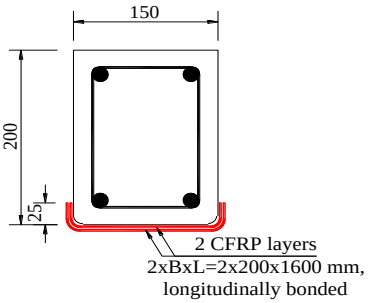

e) Cross section A-A

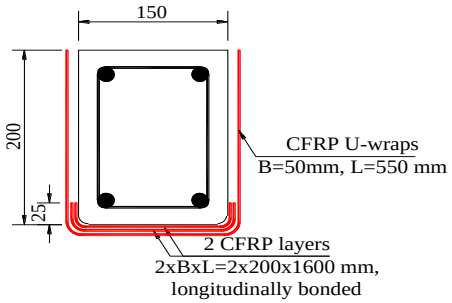

f) Cross section B-B

g) Beams after CFRP retrofitting

Figure 5. FRP retrofitting

2.4. Loading Test Setup

Figure 6 shows the experiment setup for loading tests. The beam was simply supported with a span length of 1650 mm. Three linear variable displacement transducers (LVDT), a hydraulic jack, and a load cell were used for the tests. The load cell was used to measure the force acting on the beams. Two LVDTs were installed at the two supports to measure support settlements, while the other LVDT was installed at the mid-span to measure the deflections of the tested beams. The load and deflections/settlements were simultaneously recorded during the tests. Based on the data obtained, the deflections of mid-span relative to the supports were computed. To avoid errors due to contact between RC beams and the testing system, each beam was first loaded to around 1 kN and then released to an almost zero load. After that, the main testing procedure was conducted until the beams failed.

Figure 6. Loading test setup

3. Experimental Results and Discussions

3.1. Failure Modes

Figure 7 shows the failure states of the tested beams on the testing apparatus. Among the un-retrofitted beams, beam B0 failed with the largest deflection, followed by beam B30, whereas the failure deflection of beam B60 is the smallest. Beam B0 failed in flexure, with the main cracks concentrated at the mid-span. The failure of beam B30 was almost similar to the flexural failure of beam B0. In contrast, beam B60 had flexural cracks that developed as the load increased; then, crushing of concrete occurred, followed by inclined cracks that started from this crushing point. As the load further increased, shear cracks developed and were finalized by shear failure with two shear failure surfaces, as can be seen in Figure 7-g. This can be explained by the higher reduction of concrete strength after a longer fire exposure (60 min) compared to beam B30. In contrast to the un-retrofitted beams, the deflections of the retrofitted beams were relatively small. This can be generally attributed to the presence of CFRP retrofitting, which significantly reduced the deformation, leading to low curvature and ductility in retrofitted beams. Another aspect is that the failure of CFRP retrofitted beams is associated with CFRP retrofitting, whereas the failure of control beam B0 and postfire beams B30 and B60 is associated with the yielding of steel. No rupture of the flexural CFRP was observed. This can be explained by the fact that the tensile strength of CFRP is much higher than the strength of cover concrete, which was reduced by fire. Therefore, the cover concrete became the weakest region for failure.

a) B0

b) B30

g) B60

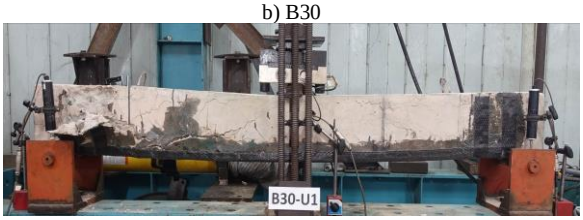

c) B30-U1

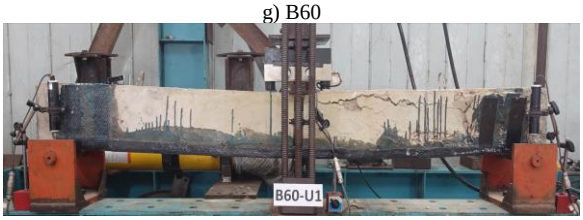

h) B60-U1

d) B30-U2

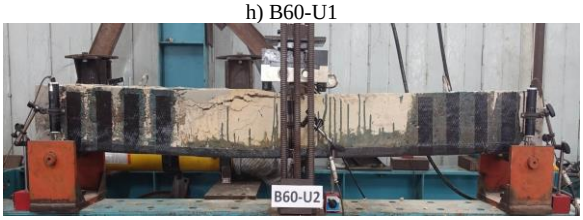

i) B60-U2

e) B30-U3

j) B60-U3

f) B30-U4

k) B60-U4

Figure 7. Failure of beams after testing

Regarding the control beam B0, tiny flexural cracks on the bottom and side surfaces in the tension zone developed at about 6 kN. As the load further increased, the widths and lengths of these cracks continued to develop and propagated upward to the center axis of the beams, while new cracks developed in a wider region. When the load was approaching the yield load, the cracks propagated beyond the center axis, and the cracking region expanded over a larger area, forming an inclined angle of about 45º. When the beam went into its plastic stage, almost no new cracks were developed, while the widths of current cracks continued to be widened. The speed of width development was fastest for the cracks close to the mid-span. As the displacement further increased in the plastic stage, the development of crack widths tended to focus on a few cracks at the mid-span. This phenomenon can be resulted from the yielding of steel. When the beam approached its ultimate stage, minor crushing of concrete occurred in the compression zone due to the large curvature of the beam.

Moving on to postfire beams B30 and B60, their crack development was generally similar to that of control beam B0 up to yielding. However, differences were observed when the tested beams were approaching the ultimate state. For beam B30, the concrete in the compression zone crushed earlier at a smaller deflection, and inclined cracks developed downward from the top side to about 1/3 the height of the beams. The difference was more pronounced for beam B60 when it approached the ultimate. The concrete in the compression zone was crushed, and inclined cracks developed. The development of cracks started at the loading point and on one support. These cracks gradually formed two parallel shear failure surfaces, as can be seen in Figure 7-g. Therefore, beam B60 failed by yielding of steel, followed by crushing of concrete in the compression zone, and finalized by shear failure. The shear failure of beam B60 can be attributed to the higher reduction in concrete strength after 60-min fire exposure.

Regarding CFRP retrofitted postfire RC beams (Figures 7-c to 7-f and 7-h to 7-k), peeling-off failure of cover concrete between U-wrap FRP and steel occurred, whereas minor concrete crushing was observed. In the vertical direction, the peeling-off started at the ends of U-wraps and quickly propagated downward. In the horizontal direction, the peeling-off progressively propagated toward the mid-span and the support. The failure sequence of B60-U group beams was generally similar to that of B30-U group beams; however, B60-U group beams had the peeling-off occurring shortly after the yielding point, and their inclined cracks were much more obvious. These differences can be attributed to the higher reduction in concrete strength due to the longer fire. The higher reduction in concrete strength shifted the beam from flexural failure to shear failure. CFRP U wraps successfully prevented the shear failure. CFRP retrofitting systems altered the failure mode in the form of yielding of steel (beams B30–B0) to the failure mode by peeling off of concrete between CFRP and steel reinforcement. This is because the strength of the concrete cover was significantly reduced by the fire.

3.2. Load–Deflection Curves

Figure 8 plots the load-deflection curves of B30-group beams in comparison with the curve of control beam B0. The same axis system limits were used for visual comparison. The yield and ultimate points and their coordinates are shown in this Figure. The coordinates of these points represent the strength and deformation capacities, which are analyzed in the subsequent sections. After the yield point, the curves deviated away from their linearity, and the nonlinearity increased as the beams approached their ultimate states. Up until yielding, the behavior of the tested beams was nearly linear. A straight line can be used to approximate the curve from zero to the yielding point. Similarly, the curve from the yielding point to the ultimate point can also be approximated by a straight line. The idealized lines are plotted in the Figure. The slopes of these straight lines before yielding and after yielding are called yield stiffness and plastic stiffness, respectively.

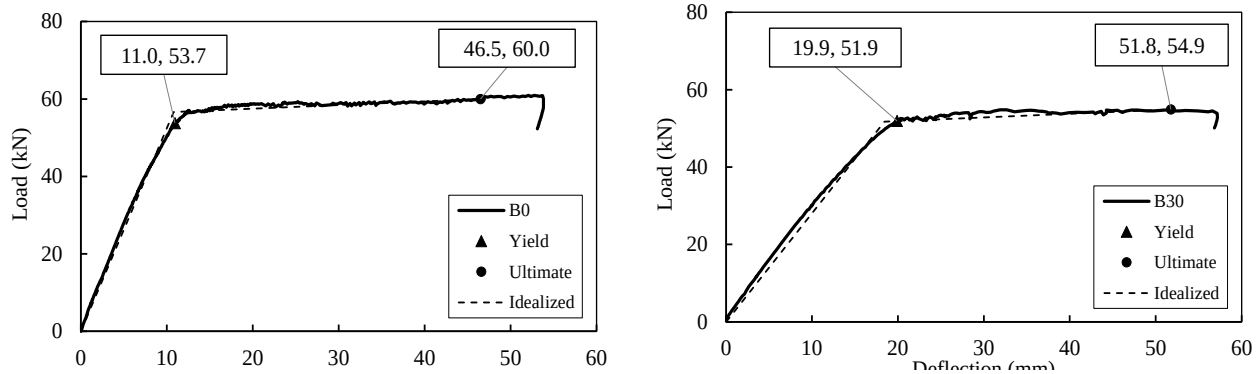

a) Beam B0

b) Beam B30

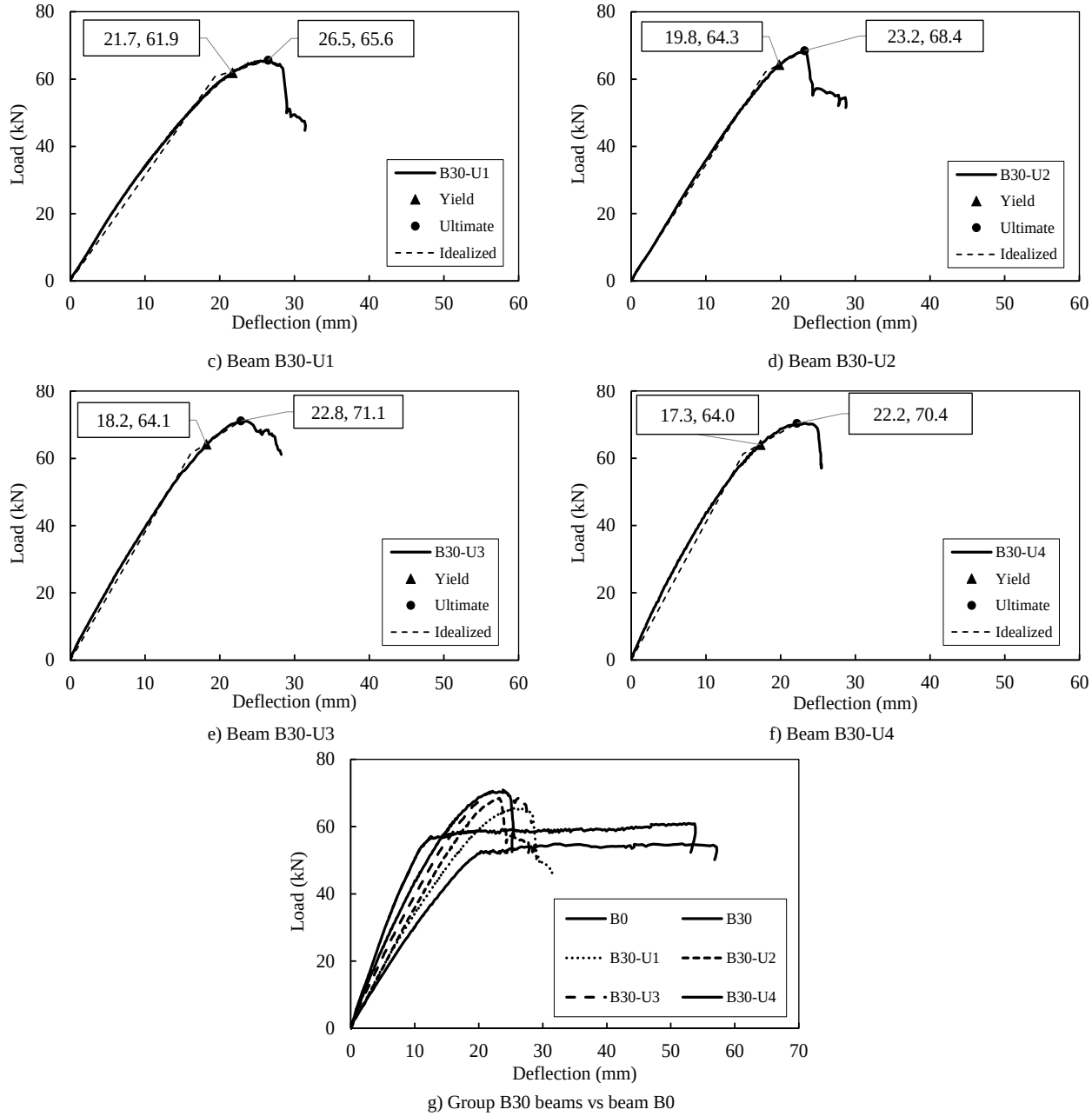

Figure 8. Load–deflection curves of beams of groups B30 and B0

Figures 8-a and 8-b show that beams B0 and B30 have similar load-deflection curves, which have a long plateau in plastic regions. However, a 30-min fire shifted the curve of B30 downward and rightward compared with the curve of beam B0. 30-min fire also shortened the plastic plateau. Interestingly, the presence of CFRP retrofitting systems greatly changed the shape of the curves of retrofitted beams B30-U1–B30-U4 (Figures 8-c to 8-f) compared with the curves of beams B30 and B0. The load-deflection curves are linear up to yielding, followed by a short nonlinear portion, and finalized by peeling-off of U-wrap FRP. The curves of beams B30-U1–B30-U4 have a longer elastic phase but a much shorter plastic phase than those of beams B30 and B0. This is attributed to the elastic behavior of CFRP until failure of the beams. No rupture of CFRP was observed during the tests. CFRP also delayed the yielding of steel and redistributed the strain in the tension and compression zones. After yielding, the strain of tension steel increased while its stress remained almost unchanged. This provides conditions that the increased amount of force after yielding was mainly resisted by the flexural CFRP. The increase in tension force of CFRP further leads to the difference in force distributed in steel and CFRP, providing a condition for the development of shear cracks in concrete between CFRP and steel. The peeling-off failure is the reason that significantly shortened the plastic phase of FRP retrofitted RC beams compared with that of un-retrofitted beams. The peeling-off failure of the concrete occurred quickly, resulting in a sharp drop in load.

Figure 8-g compares the curves of B30-group beams with the curve of control beam B0. CFRP retrofitting significantly improved the strengths (yield and ultimate loads) of CFRP retrofitted beams. CFRP retrofitting successfully enhanced the strengths of postfire RC beams compared with the strengths of control beam B0. The slope (stiffness) of retrofitted postfire RC beams was also recovered to an extent, at which it is higher than that of beam B30 but still lower than that of beam B0. This can be attributed to the reduction in strength of the cover concrete due to fire exposure.

Figures 9b to 9f plot the load-deflection curves of B60-group beams. The same phenomenon can be observed: the plastic stages of the curves are very short, and they are much shorter than the plastic stages of B30-group beams. The characteristics described in the previous paragraph become more pronounced for B60-group beams. The levels of shifting the curves were stronger. 60-min fire greatly decreased the curves of B60-group beams. This is because these beams suffer a higher reduction in concrete strength because of the longer duration of fire. A thicker layer of concrete cover experienced a reduction in strength. The higher strength reduction in a thicker layer of concrete cover resulted in earlier debonding, significantly decreasing the mechanical properties of the retrofitted beams compared with those of beam B30. This is also the reason for the lower effectiveness of the CFRP retrofitting system.

Figure 9-g compares the curves of B60-group beams with the curve of control beam B0. It can be seen that, compared with beam B60, CFRP retrofitting caused a significant increase in both load-carrying capacity and stiffness; however, CFRP retrofitting significantly reduced the ductility. The curves of retrofitted beams are still below the curve of control beam B0. Fire shifted the load-deflection curves downward and rightward. In contrast, FRP retrofits significantly altered the load-deflection behavior of postfire RC beams by shifting the curves upward and leftward. The "upward" recoverability for beams exposed to 30-min fire is very satisfactory, but that for beams exposed to 60-min fire is still lower than the curve of the control beam.

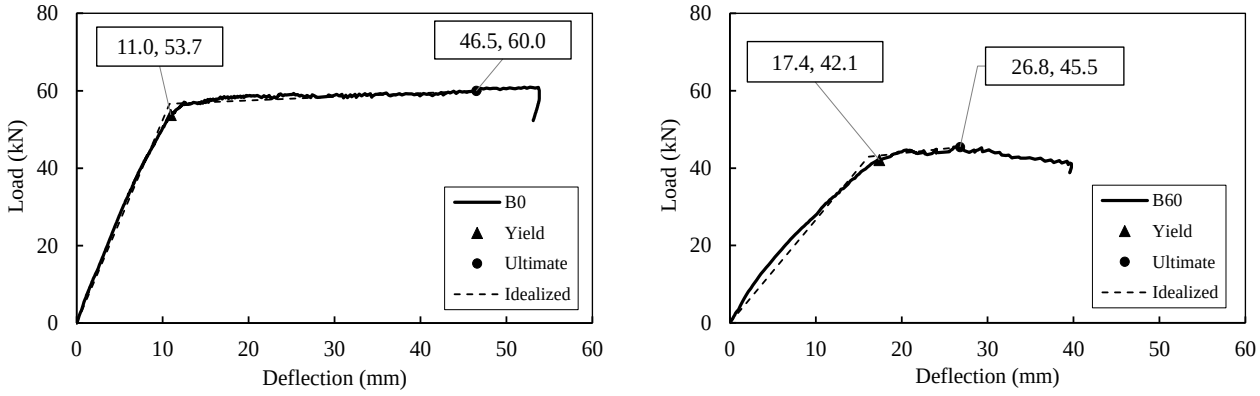

a) Beam B0

b) Beam B60

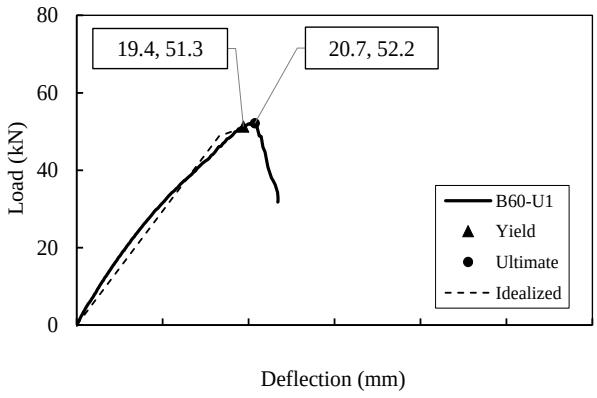

c) Beam B60-U1

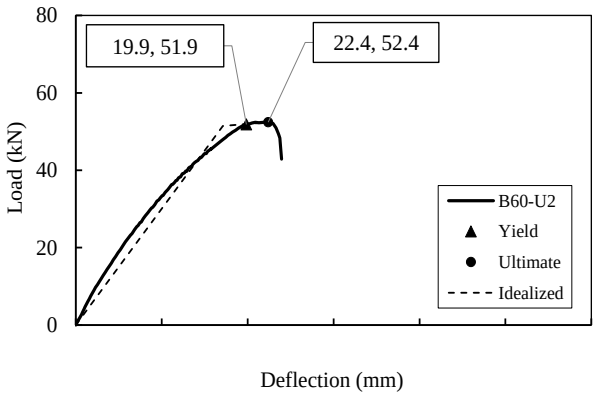

d) Beam B60-U2

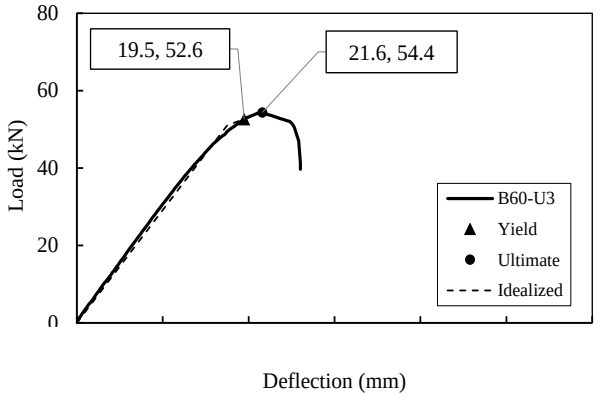

e) Beam B60-U3

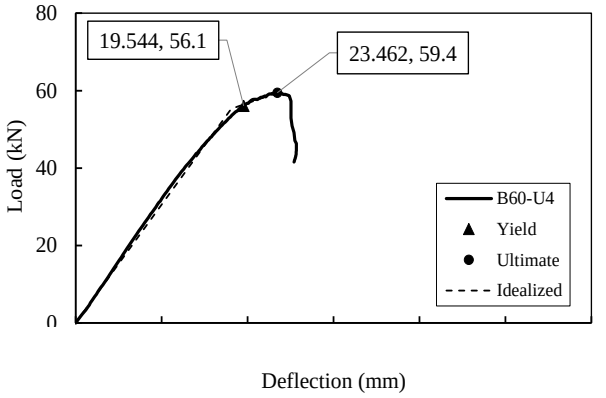

f) Beam B60-U4

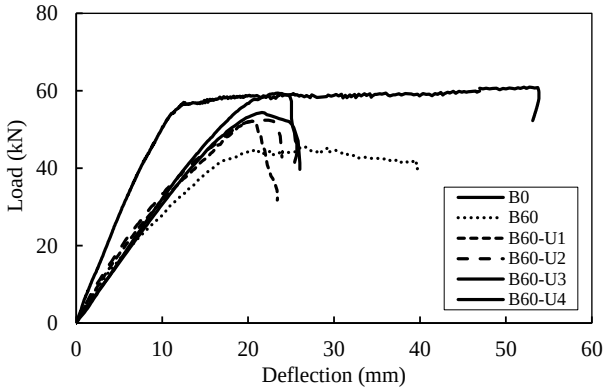

g) B60-group beams vs beam B0

Figure 9. Load–deflection curves of beams of groups B60 and B0

The effectiveness of the U-wrap CFRP slightly increased with the increase in the number of wraps. It is more pronounced in the case of a longer duration of fire because the strength of the concrete was significantly affected, which resulted in the peeling off of the concrete. The effectiveness was marginally and positively affected by the number of FRP U-wraps, whereas it was significantly and negatively affected by the fire duration. The effectiveness of FRP retrofitting increased as the number of U-wraps increased because U-wraps delayed and prevented the early peeling off of concrete.

3.3. Yield Load

The yield loads of the tested beams are displayed in Figure 10-a. The yield loads of CFRP retrofitted beams B30-U1–B30-U4 (B30-group beams) were much higher than those of control beam B0 and beam B30. In contrast, the yield loads of CFRP retrofitted beams B60-U1–B60-U4 (B60-group beams) and beam B60 were much lower than the yield load of control beam B0. The yield load of beam B60 was the lowest. Particularly, the yield load of beam B30 was 51.9 kN, which is 3.4% lower than that of control beam B0. With CFRP retrofitting, the yield loads of beams B30-U1–B30-U2 increased to 61.9 kN–64.3 kN, which is corresponding to 15.3−19.7% higher than the yield load of control beam B0. Compared with the yield load of beam B30, the yield load increased by 18.7−23.1%. This shows that FRP retrofitting is effective in recovering/increasing the yield load of RC beams exposed to 30 min of fire.

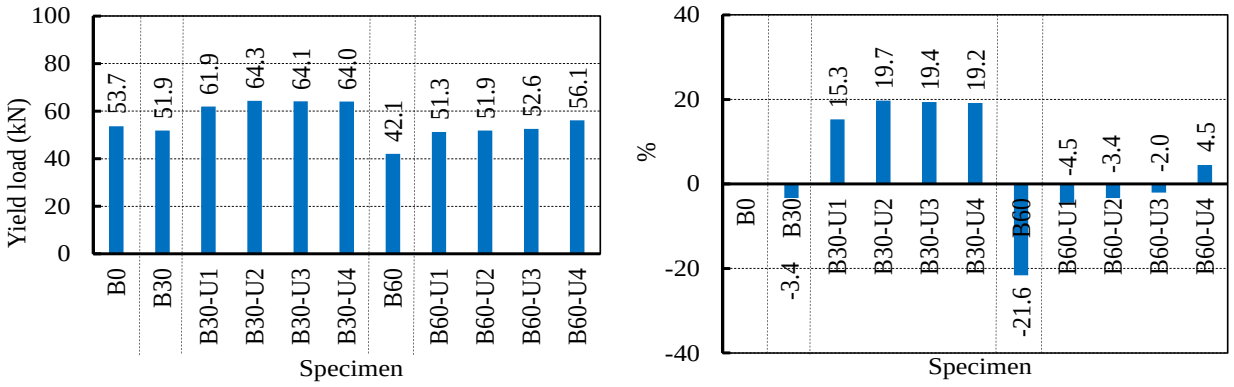

a) Yield loads b) Increase

Figure 10. Yield loads of beams

Moving on B60-group beams, fire exposure reduced the yield load of beam B60 to 42.1 kN, which is 21.6% lower than that of control beam B0. The yield loads of CFRP retrofitted beams B60-U1−B60-U3 are 51.3 kN−52.6 kN, which are 4.5−2.0% lower than the yield load of control beam B0. Thus, the retrofitting of U1-U3 almost recovered the yield load to that of control beam B0. Beam B60-U4 had a yield load of 56.1 kN, which is 4.5% higher than that of control beam B0. Overall, FRP retrofitting significantly increased the yield load of B30-group beams; however, its effectiveness was limited for B60-group beams because of the significant reduction in yield load of beam B60 caused by the longer duration of fire. With the same flexural CFRP, the increase of U wraps slightly increased the yield load of retrofitted postfire RC beams because U wraps help to increase the tensile force in the flexural CFRP, leading to the occurrence of peeling-off failure.

3.4. Yield Deflection

Figure 11-a shows the yield deflections of CFRP-retrofitted postfire beams compared with those of beams B0, B30, and B60. Figure 11-b shows the comparison of yield deflections of postfire RC beams (with and without FRP

retrofitting). The yield deflections of beams B30 and B60 were 19.9 mm and 17.4 mm, which are 80.9% and 58.2% higher than the yield deflection (11.0 mm) of control beam B0, respectively. CFRP retrofitting increased the yield deflection of beam B30-U1, whereas the increase in the number of U wraps slightly decreased the yield deflection. Beams B30-U1−B30-U4 had yield deflections of 21.7−17.3 mm, which are 97.3−57.3% higher than the yield deflection of control beam B0, respectively.

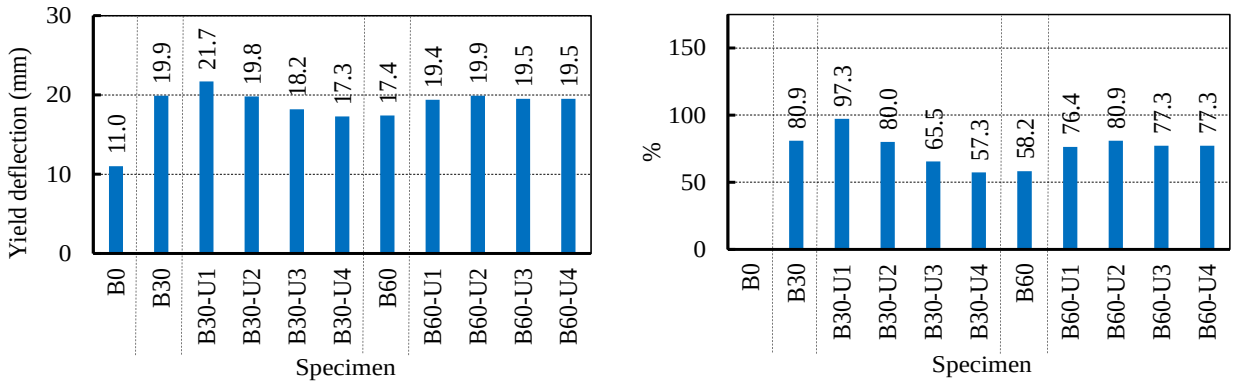

a) Yield deflections b) Increase

Figure 11. Yield deflections

Moving on beams exposed to fire for 60 min, the yield deflections of beams B60-U1−B60-U4 varied around 19.5 mm, which is about 78% higher than the yield deflection of the control beam. The CFRP U-wraps increased the bonding between the longitudinal CFRP and concrete, preventing the early debonding of the longitudinal CFRP, thus increasing the yield deflection of CFRP retrofitted postfire RC beams. The elasticity up to rupture of CFRP, the decrease in mechanical properties of materials, and the decrease in bond between steel and concrete can contribute to the increase in yield deflection of FRP retrofitted beams compared with that of the control beam.

3.5. Ultimate Load

The ultimate loads of the tested beams are shown in Figure 12-a. Control beam B0 had an ultimate load of 60.0 kN, which was reduced to 54.9 kN and 45.5 kN after exposure to fire for 30 min and 60 min, respectively. These reductions correspond to 8.5% and 24.2% compared with the ultimate load of control beam B0. The ultimate loads of B30-U1–B30-U4 beams varied from 65.6 kN–71.1 kN, which are 9.3−18.5% higher than those of control beam B0. This shows the capability of CFRP retrofitting to recover and increase the strength of postfire beams.

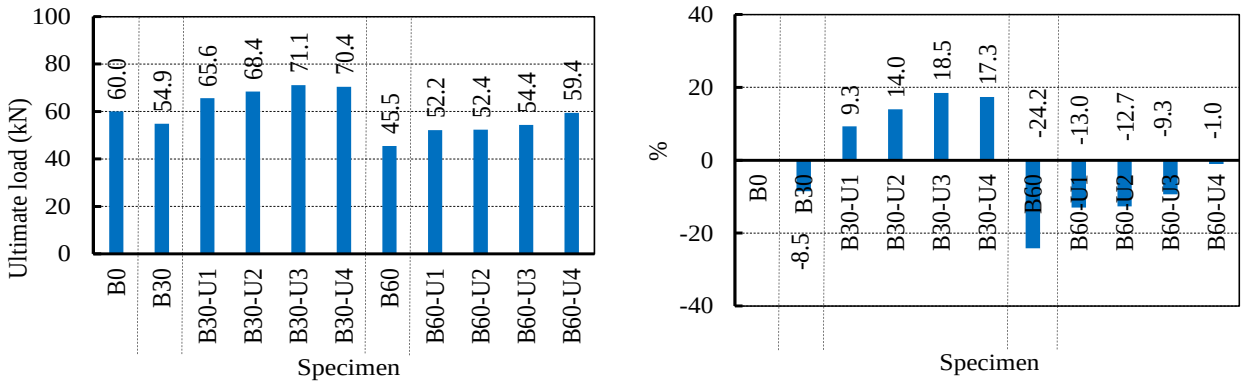

a) Ultimate loads b) Increase

Figure 12. Ultimate loads

Moving on to group B60, the ultimate loads of B60-group beams varied from 52.2 kN to 59.4 kN, which are 13.0−1.0% lower than the ultimate load of control beam B0. The ultimate load of beam B60-U4 was almost equal to that of control beam B0, showing that CFRP retrofitting with a higher number of U wraps can be more effective in recovering the strength of RC beams exposed to longer fire durations. Figure 12 also indicates that the higher number of U wraps increased the effectiveness of CFRP retrofitting, although the same flexural CFRP amount was used. This can be attributed to the decrease in concrete strength, whereas the higher number of U-wraps tends to delay the debonding.

3.6. Ultimate Deflection

The deflections at the ultimate states of the tested beams are shown in Figure 13-a. Figure 13-b compares the ultimate deflections of un-retrofitted and CFRP-retrofitted postfire RC beams with the ultimate deflection of control beam B0. The control beam B0 had an ultimate deflection of 46.5 mm, whereas CFRP-retrofitted beams had much lower ultimate deflections. Beam B30 had an ultimate deflection of 51.8 mm, which increased by 11.4% compared with control beam B0. Beam B60 had an ultimate deflection of 26.8 mm, which is 42.4% lower than that of control beam B0.

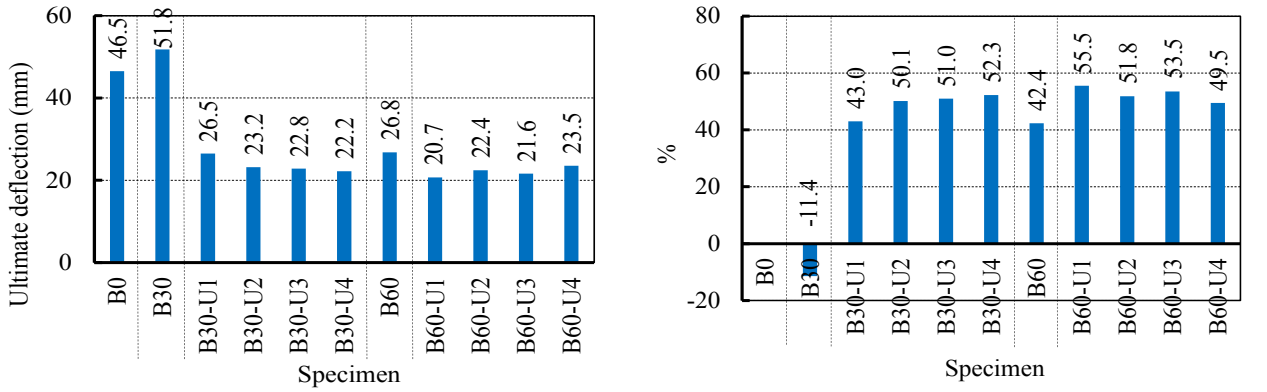

a) Ultimate deflections b) Increase

Figure 13. Ultimate deflections

Ultimate deflections of postfire RC beams were further decreased by the presence of CFRP retrofitting. Beams B30-U1−B30-U4 had ultimate deflections varying from 22.2 mm to 26.5 mm, which decreased by 43.0−52.3% compared with control beam B0. The ultimate deflections of beams B60-U1–B60-U4 varied from 20.7 mm to 23.5 mm, which are 55.5−49.5% less than the ultimate deflection of control beam B0. Overall, the reduction in ultimate deflections includes the two following stages. First, fire caused a significant reduction in ultimate deflections, which is attributed to the negative change in the mechanical properties of materials. Then, FRP retrofitting further reduced the ultimate deflection by the peeling-off failure.

3.7. Yield Stiffness

The stiffness of the tested beams is plotted in Figure 14-a, and it is compared with the stiffness of control beam B0 as shown in Figure 14-b. The stiffness of control beam B0 was highest at 5.24 kN/mm. The stiffness of beams B30 and B60 was reduced to 2.81 kN/mm and 2.66 kN/mm, which are 46.4% and 49.2% less than that of the control beam, respectively. The stiffness of postfire beams retrofitted with CFRP slightly increased compared with that of postfire beams B30 and B60; however, the stiffness of these beams was not completely recovered from that of control beam B0. The stiffness of beams B30-U1–B30-U4 varied from 3.14 kN/mm to 4.09 kN/mm, which is 40.1% to 21.9% lower than that of control beam B0, respectively. The stiffness of beams B60-U1–B60-U4 varied from 2.95 kN/mm to 3.06 kN/mm, which is 43.7−41.6% less than that of control beam B0. Another aspect that can be observed from Figure 14 is that the increase in U wraps increased the stiffness of CFRP retrofitted postfire RC beams.

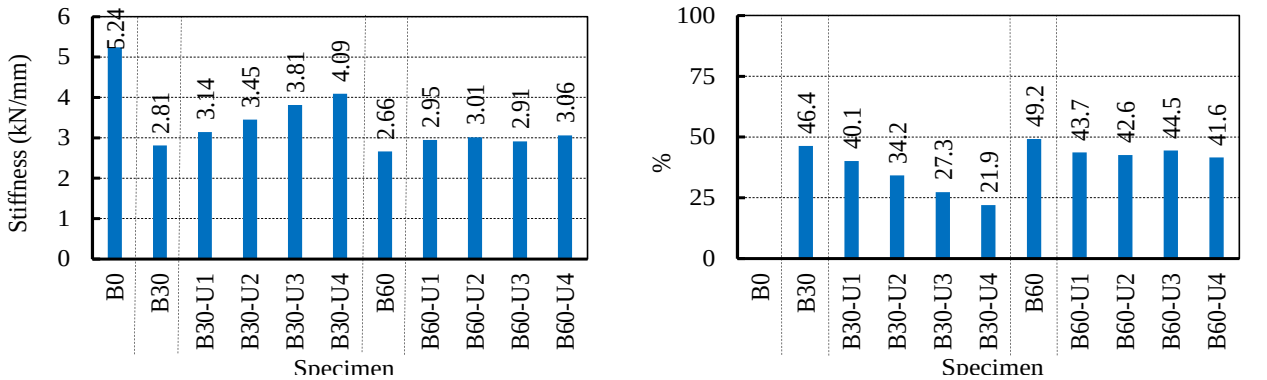

a) Stiffness b) Increase

Figure 14. Stiffness

3.8. Ductility

The ductility of tested beams was computed as the ratio of ultimate deflections (presented in Section 3.6) to yield deflections (presented in Section 3.4), and the results are shown in Figure 15. The ductility of control beam B0 was 4.23, classified as high ductility, according to ASCE/SEI 41–17 [49]. However, 30-min and 60-min fires significantly decreased the ductility of beams B30 and B60 to 2.60 and 1.54, which are 38.5% and 63.6% lower than that of the control beam, respectively. Beams B30 and B60 are thus classified as ‘moderate ductility’ and ‘low ductility’ [49], respectively. Fire increased the yield deflection, whereas it significantly decreased the ultimate deflection; consequently, the ductility significantly decreased. CFRP retrofitting further reduced the ductility of retrofitted beams of groups B30 and B60 to lower values of 1.07−1.28, which are 69.7−74.7% lower than the ductility of the control beam. Although these ductility values classified these beams as ‘low ductility’ [49], these values are close to 1, and thus they are very close to brittle behavior. This low ductile behavior can be explained by the failure modes of these beams, which are

attributed to the peeling-off of concrete because the concrete around the beams was exposed to fire and suffered a significant reduction in strength. The 'low ductile' behavior of these CFRP retrofitted postfire beams is a drawback of CFRP retrofitting. Further investigations should be carried out to improve the mechanical properties of postfire concrete and increase the ductility of these beams.

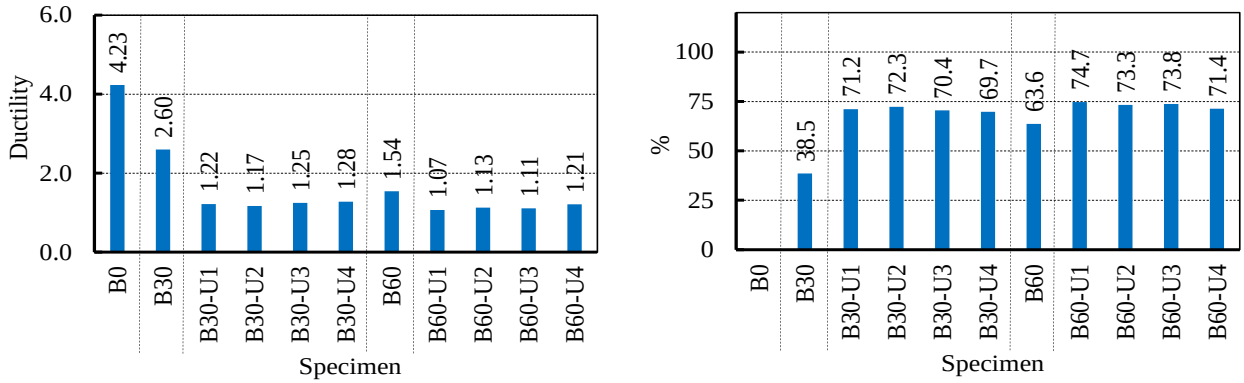

a) Ductility b) Increase

Figure 15. Ductility

4. Theoretical Model

As observed and described in Section 3.1, no shear failure occurred on FRP retrofitted postfire RC beams. Therefore, it can be concluded that U-wrap CFRP successfully prevents the shear failure of FRP retrofitted postfire RC beams. In addition, the increase in the number of U wraps slightly increases the load-carrying capacity, as presented in Sections 3.3 and 3.5. For the sake of simplification, it can be assumed that the flexural CFRP contributes to the flexural resistance while the U wraps contribute to the shear resistance.

A typical cross section of postfire beams retrofitted with FRP is shown in Figure 16-a. The 500°C isotherm line x_{500} (the dashed line) is also shown in this Figure, and this isotherm line divided the section into two parts by the outer and inner areas. The longitudinal FRP can be divided into FRP bonded on the bottom surface (A^b_{frp}) and FRP on the two side surfaces (A^s_{frp}). Plane strain distribution of cross section is adopted and is shown in Figure 16-b. Figure 16-c shows tensile forces of FRP and steel and the compressive stress on concrete. Figure 16-d shows the equivalent stress block of concrete, and its total compressive force (C_c) is shown in Figure 16-e.

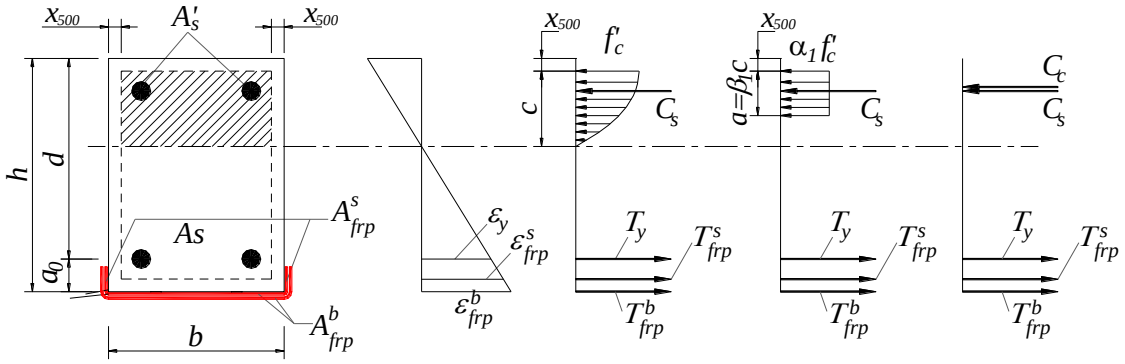

(a) (b) (c) (d) (e)

Figure 16. Theoretical analyzes of beam sections

Three tensile forces:

1) The tensile force of steel bars T_s is computed by Equation 1. When $f_s = f_y$, $T_s = T_y$. In other words, T_y is the yield tensile force of steel bars;
2) The tensile force of bottom FRP T^b_{frp} is computed by Equation 2;
3) The tensile force of side FRP T^s_{frp} is computed by Equation 3;

Two compressive forces:

1) The compressive force of steel (C_s) is expressed Equation 4;
2) The compressive forces of concrete (C_c) is expressed by Equation 5;

where f_s and A_s are the stress and area of tensile steel, respectively; f^b_{frp} and f^s_{frp} are stresses of CFRP at bottom and side

surfaces, respectively, f_s' and A_s' are the stress and area of compressive steel; f_c' is the concrete strength; $a = \beta_1 c$ and $0.85f_c'$ is the depth and stress of the equivalent stress block; *b'* is the width of the cross section within the 500°C isotherm lines, calculated by Equation 6, where x_{500} (m) is the depth measured from the surface to the 500°C isotherm lines.

The 500°C isotherm depth x_{500} (m) based on the Wickstrom's model [50] of temperature distribution is calculated by Equation 7, as suggested by Purkiss & Li [51]. In Equation 7, α_r is ratio of the thermal diffusivity to the reference value of 0.417×10^{-6} m^2/s [52]; *t* is the fire duration in hours; n_w is the ratio of the fire temperature to the temperature of concrete, calculated by Equation 8; *T* is the fire temperature determined by Equation 9 based on the ISO-834 fire:

$$T_s = f_s A_s \quad (1)$$

$$T_{frp}^b = f_{frp}^b A_{frp}^b \quad (2)$$

$$T_{frp}^s = f_{frp}^s A_{frp}^s \quad (3)$$

$$C_s = A_s^{'} f_s^{'} \quad (4)$$

$$C_c = 0.85 f_c^{'} a b^{'} \quad (5)$$

$$b^{'} = b - 2x_{500} \quad (6)$$

$$x_{500} = \sqrt{\frac{\alpha_r t}{exp\left(4.5 + \frac{480}{0.18 n_w T}\right)}} \quad (7)$$

$$n_w = 1 - 0.0616 t^{-0.88} \quad (8)$$

$$T = 20 + 345 \times log(8 \times 60 \times t + 1) \quad (9)$$

The 500°C isotherm depths x_{500} for 30 and 60 min of fire are 12.5 mm and 23.4 mm, respectively. The tensile forces T_s, T_{frp}^b, and T_{frp}^s have the lever arms with respect to the centroid of the equivalent compressive stress block are calculated by Equations 10 to 12, respectively, where *h* is the cross-sectional height; a_0 is the thickness of concrete cover calculated from the centroid of tensile steel; $d = h - a_0$ is the effective depth of the tensile steel; a_s is the distance from the centroid of side CFRP to bottom surface; *c* is the depth to the neutral axis:

$$jd = d - 0.5a - x_{500} = h - a_0 - 0.5a - x_{500} \quad (10)$$

$$kh^b = h - 0.5a - x_{500} \quad (11)$$

$$kh^s = h - 0.5a - a_s - x_{500} \quad (12)$$

Due to its location in the concrete compression zone, the lever arm of compressive steel force is relatively small and its bending moment with respect to the compressive concrete block's center can be ignored. Equation 13 shows the bending moments of CFRP retrofitted sections with respect to the center of the equivalent concrete stress block.

$$M_y = T_s jd + T_{frp}^b kh^b + T_{frp}^s kh^s \quad (13)$$

Equation 14 shows the equilibrium condition while Equation 15 shows the equilibrium at yield ($T_s = A_s f_y$). The depth *a* is thus found by Equation 16.

$$C_c + C_s = T_s + T_{frp}^b + T_{frp}^s \quad (14)$$

$$0.85 f_c^{'} a b^{'} + A_s^{'} f_s^{'} = A_s f_y + A_{frp}^b f_{frp}^b + A_{frp}^s f_{frp}^s \quad (15)$$

$$a = \frac{A_s f_y - A_s^{'} f_s^{'} + A_{frp}^b f_{frp}^b + A_{frp}^s f_{frp}^s}{0.85 f_c^{'} b^{'}} \quad (16)$$

Equations 17 and 18 are used to calculate the stresses in bottom and side CFRP, respectively, where ε_{frp}^b and ε_{frp}^s are strains of FRP bonded on bottom and side surfaces, respectively, and E_{frp}= 240 GPa is the modulus of CFRP.

$$f_{frp}^b = \varepsilon_{frp}^b E_{frp} \quad (17)$$

$$f_{frp}^s = \varepsilon_{frp}^s E_{frp} \quad (18)$$

Similar triangles in Figure 16-b are used to obtain Equations 19 to 21. In this work, $\varepsilon_m = 0.003$ [53], which is the concrete strain at the top fibre, is adopted.

$$\frac{c}{d-(c+x_{500})} = \frac{0.003}{\varepsilon_y} \quad (19)$$

$$\frac{d-(c+x_{500})}{h-(c+x_{500})} = \frac{\varepsilon_y}{\varepsilon_{frp}^b} \quad (20)$$

$$\frac{d-(c+x_{500})}{h-(c+x_{500})-a_s} = \frac{\varepsilon_y}{\varepsilon_{frp}^s} \quad (21)$$

The depth *c* is computed by Equation 22 by rearranging Equation 19. After having the depth *c*, the strains of bottom and side CFRPs are calculated by Equations 23 and 24, which are the arrangements of Equations 20 and 21, respectively. Yield bending moment (Equation 25) is computed as the total moment of tensile forces with respect to the center of the equivalent stress block. This model can also be used for the case of un-retrofitted postfire RC beams by eliminating the second and third terms of Equation 25.

$$c = \frac{d-x_{500}}{1+\frac{\varepsilon_y}{0.003}} = \frac{d-x_{500}}{1+r} \quad (22)$$

$$\varepsilon_{frp}^b = \frac{\varepsilon_y(h-(c+x_{500}))}{d-(c+x_{500})} \quad (23)$$

$$\varepsilon_{frp}^s = \frac{\varepsilon_y(h-(c+x_{500})-a_s)}{d-(c+x_{500})} \quad (24)$$

$$M_y = A_s f_y(d-0.5a-x_{500}) + A_{frp}^b f_{frp}^b(h-0.5a-x_{500}) + A_{frp}^s f_{frp}^s(h-0.5a-a_s-x_{500}) \quad (25)$$

Yield moments predicted by this model and those of experiments were presented and compared in Table 2. Because the model does not account for the effect of CFRP U wraps; therefore, the predicted values of yield moment for four retrofitting cases of different number of U wraps are the same. This is a limitation of the model because it is difficult to account for the effect of U wraps. However, it is interesting to closely examine the experimental values, which vary from 25.5 kNm to 26.5 kNm for group B30-U and from 21.2 kNm to 23.1 kNm for group B60-U. The difference of these values of group B30 beams is only (26.5−25.5)/25.5×100% = 3.9%. Similarly, the difference of group B60 beams is about (23.1−21.2)/21.2×100% = 9%. These show a negligible effect of U wraps on the load-carrying capacity of FRP retrofitted postfire beams.

Table 2. Comparisons of yield moments

Beam	Group	x_{500} (mm)	*a* (mm)	Yield moment (kNm)		Difference (%)
				Analysis	Experiment	
B0	B-0	0	6.5	22.1	22.2	-0.5
B30	B30	12.5	0.0	20.8	21.4	-2.8
B30-U1		12.5	14.2	26.5	25.5	3.9
B30-U2		12.5	14.2	26.5	26.5	0.0
B30-U3		12.5	14.2	26.5	26.4	0.4
B30-U4		12.5	14.2	26.5	26.4	0.4
B60	B60	23.4	0.0	19.3	17.4	10.9
B60-U1		23.4	15.7	24.6	21.2	16.0
B60-U2		23.4	15.7	24.6	21.4	15.0
B60-U3		23.4	15.7	24.6	21.7	13.4
B60-U4		23.4	15.7	24.6	23.1	6.5

Specifically, beam B0 has a predicted yield moment of 22.1 kN.m, which is almost similar to the experimental yield moment. Moving on to group B30 beams, the predicted yield moments of beam B30 are 20.8 kN.m which is 2.8% lower than the experimental value. The predicted yield moment of beams B30-U1 – B30-U4 is 26.5 kN.m while the experimental yield moments of these beams vary from 25.5 kN.m to 26.4 kN.m., and the difference is thus less than 3.9%. For beam B60, the predicted yield moment is 19.3 kN.m, which is 10.9% higher than the experimental yield moment. For group B60 beams, the predicted yield moment of CFRP retrofitted beams is 24.6 kN.m, whereas the experimental yield moment varies from 21.2 kN.m to 23.1 kN.m. Thus, the difference between the two results is 16.0%. This relatively large difference can be attributed to the reduction in mechanical properties of cover concrete, which governs the peeling-off of the concrete, whereas it was not taken into account in the model. Further study should be encouraged to recover the mechanical properties of concrete, which in turn will delay or prevent the peelling-off failure.

5. Conclusions

Conclusions can be drawn as follows:

- Fire shifted the flexure failure of the control RC beam to the flexure-shear failure of postfire RC beams. The shift was more pronounced with longer fires. CFRP retrofitted postfire RC beams failed by peeling off of concrete between the U-wrap FRP and concrete, whereas both flexural and shear FRP did not experience any rupture. CFRP U wrapping successfully prevented the shear failure and delayed the peeling-off failure. The peeling-off started at a U wrap and progressively propagated to adjacent U wraps. The delay in peeling off was more pronounced as the number of U-wraps increased. These failure features can be attributed to the significant reduction in strength of the concrete cover.
- Fire shifted the load-deflection curves downward and rightward, whereas FRP retrofitting shifted these curves upward and leftward. Compared with the control beam and postfire beams, CFRP-retrofitted postfire RC beams had a longer elastic phase but a much shorter plastic plateau. The longer elastic phase is explained by the fact that CFRP delayed the yielding of steel by sharing the tension force, while the much shorter plastic plateau is explained by the peeling-off failure. A longer fire resulted in the earlier peeling off due to the higher reduction in concrete strength.
- CFRP retrofitting considerably increased the yield deflection by 58.2−97.3% but decreased the ultimate deflection capacity by 43.0−55.5% compared with the control beam. Consequently, the ductility of CFRP retrofitted postfire RC beams was reduced by 69.7−74.7% compared with that of the control beam, and the ductility was close to 1, categorized as 'low ductility' and close to 'brittle failure'. The ultimate state of the tested beams was governed by the peeling-off failure that occurred shortly after the yielding of tensile steel. The peeling-off failure and its progressive occurrence caused a sharp drop in load. The non-ductile and progressive characteristics can be considered drawbacks of the retrofitting technique, which need further studies to address these issues.
- CFRP retrofitting was able to recover the load-carrying capacity diminished by the 60-min fire, and it successfully increased the load-carrying capacity of 30-min postfire beams by up to 23.1% compared with that of the control beam. Fire significantly decreased the stiffness of postfire beams by 46.4−49.2% compared with that of the control beam. CFRP retrofitting did not completely recover the stiffness of 30-min postfire beams, e.g., at least 21.9% lower than the stiffness of the control beam, whereas it marginally recovered the stiffness loss of 60-min postfire beams. The fire duration importantly governed the mechanical properties and the FRP retrofitting effectiveness of postfire RC beams via the decrease in strength of cover concrete.
- The load-carrying capability of CFRP retrofitted postfire beams can be predicted using the analytical model, which was developed based on the fire duration and a model of temperature distribution in concrete. In contrast to the infeasibility of obtaining temperature distribution in concrete in a real fire event, the feasibility of obtaining fire duration makes the model viable for practical use. The simplicity, practicability, and reasonable accuracy of the proposed model can make it a useful tool for structural engineers in practice.

As observed in the experiments, the concrete cover, which was exposed to fire and suffered a significant reduction in strength, played a critical role and governed the failure and behavior of CFRP retrofitted postfire RC beams. Further studies should be carried out to address this issue. For example, improving the strength of the concrete of postfire RC beams seems vital to the effectiveness of FRP due to the bond between concrete and FRP. Removing the concrete cover and replacing it with a layer of special materials before applying the FRP retrofitting can also be a research direction to address the above-mentioned issue.

6. Declarations

6.1. Author Contributions

Conceptualization, V.N.N. and V.V.C.; methodology, V.V.C.; formal analysis, V.N.N. and V.V.C.; investigation, V.N.N. and V.V.C.; resources, V.V.C.; writing—original draft preparation, V.N.N.; writing—review and editing, V.N.N. and V.V.C.; visualization, V.N.N.; supervision, V.V.C. All authors have read and agreed to the published version of the manuscript.

6.2. Data Availability Statement

The data presented in this study are available in the article.

6.3. Funding

The authors received no financial support for the research, authorship, and/or publication of this article.

6.4. Acknowledgements

The authors acknowledge Ho Chi Minh City University of Technology (HCMUT), VNU-HCM for supporting this study.

6.5. Conflicts of Interest

The authors declare no conflict of interest.

7. References

[1] Shakib, H., Zakersalehi, M., Jahangiri, V., & Zamanian, R. (2020). Evaluation of PLASCO Building fire-induced progressive collapse. Structures, 28, 205–224. doi:10.1016/j.istruc.2020.08.058.

[2] Ada, M., Sevim, B., Yüzer, N., & Ayvaz, Y. (2018). Assessment of damages on a RC building after a big fire. Advances in Concrete Construction, 6(2), 177–197. doi:10.12989/acc.2018.6.2.177.

[3] Behnam, B. (2019). Fire Structural Response of the Plasco Building: A Preliminary Investigation Report. International Journal of Civil Engineering, 17(5), 563–580. doi:10.1007/s40999-018-0332-x.

[4] Ahmadi, M. T., Aghakouchak, A. A., Mirghaderi, R., Tahouni, S., Garivani, S., Shahmari, A., & Epackachi, S. (2020). Collapse of the 16-Story PLASCO Building in Tehran due to Fire. Fire Technology, 56(2), 769–799. doi:10.1007/s10694-019-00903-y.

[5] Saadatmanesh, H., Ehsani, M. R., & Jin, L. (1997). Repair of earthquake-damaged RC columns with FRP wraps. ACI Structural Journal, 94(2), 206–X. doi:10.14359/474.

[6] Van Cao, V., & Pham, S. Q. (2019). Comparison of CFRP and GFRP Wraps on Reducing Seismic Damage of Deficient Reinforced Concrete Structures. International Journal of Civil Engineering, 17(11), 1667–1681. doi:10.1007/s40999-019-00429-y.

[7] ACI 440.2R-17. (2017). Guide for the design and construction of externally bonded FRP systems for strengthening concrete American Concrete Institute (ACI), Michigan, United States.

[8] Lam, L., & Teng, J. G. (2003). Design-oriented stress–strain model for FRP-confined concrete. Construction and Building Materials, 17(6–7), 471–489. doi:10.1016/s0950-0618(03)00045-x.

[9] Zeng, J. J., Lin, G., Teng, J. G., & Li, L. J. (2018). Behavior of large-scale FRP-confined rectangular RC columns under axial compression. Engineering Structures, 174, 629–645. doi:10.1016/j.engstruct.2018.07.086.

[10] Shayanfar, J., Kafshgarkolaei, H. J., Barros, J. A. O., & Rezazadeh, M. (2023). Unified strength model for FRP confined heat-damaged circular and square concrete columns. Composite Structures, 307(116647). doi:10.1016/j.compstruct.2022.116647.

[11] Ibrahim, M., Wakjira, T., & Ebead, U. (2020). Shear strengthening of reinforced concrete deep beams using near-surface mounted hybrid carbon/glass fibre reinforced polymer strips. Engineering Structures, 210, 110412. doi:10.1016/j.engstruct.2020.110412.

[12] Zhang, S. S., Jedrzejko, M. J., Ke, Y., Yu, T., & Nie, X. F. (2023). Shear strengthening of RC beams with NSM FRP strips: Concept and behavior of novel FRP anchors. Composite Structures, 312(116790). doi:10.1016/j.compstruct.2023.116790.

[13] Godat, A., Hammad, F., & Chaallal, O. (2020). State-of-the-art review of anchored FRP shear-strengthened RC beams: A study of influencing factors. Composite Structures, 254, 112767. doi:10.1016/j.compstruct.2020.112767.

[14] Zhang, S. S., Ke, Y., Smith, S. T., Zhu, H. P., & Wang, Z. L. (2021). Effect of FRP U-jackets on the behavior of RC beams strengthened in flexure with NSM CFRP strips. Composite Structures, 256(113095). doi:10.1016/j.compstruct.2020.113095.

[15] Jacobs, R. R., & Williams, C. S. (2023). Evaluation of flexural strengthening methods for beams with simulated deterioration using spike-anchored FRP externally bonded sheets and near-surface-mounted strips. Composite Structures, 305, 116463. doi:10.1016/j.compstruct.2022.116463.

[16] Norris, T., Saadatmanesh, H., & Ehsani, M. R. (1997). Shear and Flexural Strengthening of R/C Beams with Carbon Fiber Sheets. Journal of Structural Engineering, 123(7), 903–911. doi:10.1061/(asce)0733-9445(1997)123:7(903).

[17] Lao, X., Han, X., Ji, J., & Chen, B. (2019). The compression behavior of CFRP-repaired damaged square RC columns. Construction and Building Materials, 223, 1154–1166. doi:10.1016/j.conbuildmat.2019.07.182.

[18] Ozcan, O., Binici, B., Canbay, E., & Ozcebe, G. (2010). Repair and strengthening of reinforced concrete columns with CFRPs. Journal of Reinforced Plastics and Composites, 29(22), 3411–3424. doi:10.1177/0731684410376332.

[19] Balsamo, A., Colombo, A., Manfredi, G., Negro, P., & Prota, A. (2005). Seismic behavior of a full-scale RC frame repaired using CFRP laminates. Engineering Structures, 27(5), 769–780. doi:10.1016/j.engstruct.2005.01.002.

[20] Ahmad, H., Hameed, R., Riaz, M. R., & Gillani, A. A. (2018). Strengthening of concrete damaged by mechanical loading and elevated temperature. Advances in Concrete Construction, 6(6), 645–658. doi:10.12989/acc.2018.6.6.645.

[21] Sharif, A., Al-Sulaimani, G. J., Basunbul, I. A., Baluch, M. H., & Ghaleb, B. N. (1994). Strengthening of initially loaded reinforced concrete beams using FRP plates. ACI Structural Journal, 91(2), 160–168. doi:10.14359/4594.

[22] Al-Abdwais, A. H., & Al-Mahaidi, R. S. (2020, October). Performance of reinforced concrete beams strengthened with NSM CFRP composites for flexure using cement-based adhesives. Structures, 27, 1446-1457. doi:10.1016/j.istruc.2020.07.047.

[23] Al-Mahmoud, F., Castel, A., & François, R. (2012). Failure modes and failure mechanisms of RC members strengthened by NSM CFRP composites–Analysis of pull-out failure mode. Composites Part B: Engineering, 43(4), 1893-1901. doi:10.1016/j.compositesb.2012.01.020.

[24] Ke, Y., Zhang, S. S., Nie, X. F., Yu, T., Yang, Y. M., & Jedrzejko, M. J. (2022). Finite element modelling of RC beams strengthened in flexure with NSM FRP and anchored with FRP U-jackets. Composite Structures, 282, 115104. doi:10.1016/j.compstruct.2021.115104.

[25] Zolfaghari, S., Mostofinejad, D., Fantuzzi, N., Luciano, R., & Fabbrocino, F. (2023). Experimental evaluation of FRP-concrete bond using externally-bonded reinforcement on grooves (EBROG) method. Composite Structures, 310, 116693. doi:10.1016/j.compstruct.2023.116693.

[26] Sanginabadi, K., Yazdani, A., Mostofinejad, D., & Czaderski, C. (2022). Bond behavior of FRP composites attached to concrete using EBROG method: A state-of-the-art review. Composite Structures, 299, 116060. doi:10.1016/j.compstruct.2022.116060.

[27] Arduini, M., & Nanni, A. (1997). Behavior of Precracked RC Beams Strengthened with Carbon FRP Sheets. Journal of Composites for Construction, 1(2), 63–70. doi:10.1061/(asce)1090-0268(1997)1:2(63).

[28] Spadea, G., Bencardino, F., & Swamy, R. N. (1998). Structural Behavior of Composite RC Beams with Externally Bonded CFRP. Journal of Composites for Construction, 2(3), 132–137. doi:10.1061/(asce)1090-0268(1998)2:3(132).

[29] Buyukozturk, O., & Hearing, B. (1998). Failure Behavior of Precracked Concrete Beams Retrofitted with FRP. Journal of Composites for Construction, 2(3), 138–144. doi:10.1061/(asce)1090-0268(1998)2:3(138).

[30] Bonacci, J. F., & Maalej, M. (2000). Externally bonded fiber-reinforced polymer for rehabilitation of corrosion damaged concrete beams. ACI Structural Journal, 97(5), 703–711. doi:10.14359/8805.

[31] Al-Saidy, A. H., Al-Harthy, A. S., Al-Jabri, K. S., Abdul-Halim, M., & Al-Shidi, N. M. (2010). Structural performance of corroded RC beams repaired with CFRP sheets. Composite Structures, 92(8), 1931–1938. doi:10.1016/j.compstruct.2010.01.001.

[32] Bonacci, J. F., & Maalej, M. (2001). Behavioral Trends of RC Beams Strengthened with Externally Bonded FRP. Journal of Composites for Construction, 5(2), 102–113. doi:10.1061/(asce)1090-0268(2001)5:2(102).

[33] Rahimi, H., & Hutchinson, A. (2001). Concrete Beams Strengthened with Externally Bonded FRP Plates. Journal of Composites for Construction, 5(1), 44–56. doi:10.1061/(asce)1090-0268(2001)5:1(44).

[34] White, T. W., Soudki, K. A., & Erki, M.-A. (2001). Response of RC Beams Strengthened with CFRP Laminates and Subjected to a High Rate of Loading. Journal of Composites for Construction, 5(3), 153–162. doi:10.1061/(asce)1090-0268(2001)5:3(153).

[35] Malek, A. M., & Patel, K. (2002). Flexural Strengthening of Reinforced Concrete Flanged Beams with Composite Laminates. Journal of Composites for Construction, 6(2), 97–103. doi:10.1061/(asce)1090-0268(2002)6:2(97).

[36] Benjeddou, O., Ouezdou, M. B., & Bedday, A. (2007). Damaged RC beams repaired by bonding of CFRP laminates. Construction and Building Materials, 21(6), 1301–1310. doi:10.1016/j.conbuildmat.2006.01.008.

[37] Jeevan, N., & Jagannatha Reddy, H. N. (2018). Strengthening of RC beams using externally bonded laminate (EBL) technique with end anchorages under flexure. Asian Journal of Civil Engineering, 19(3), 263–272. doi:10.1007/s42107-018-0022-7.

[38] Al-Ghrery, K., Al-Mahaidi, R., Kalfat, R., Oukaili, N., & Al-Mosawe, A. (2022). Externally Bonded CFRP for Flexural Strengthening of RC Beams with Different Levels of Soffit Curvature. Journal of Composites for Construction, 26(1), 1176. doi:10.1061/(asce)cc.1943-5614.0001176.

[39] Choi, K. S., Lee, D., You, Y. C., & Whan Han, S. (2022). Long-term performance of 15-year-old full-scale RC beams strengthened with EB FRP composites. Composite Structures, 299, 116055. doi:10.1016/j.compstruct.2022.116055.

[40] Li, G., Zhang, A., Jin, W., Xiao, Y., & Li, H. (2023). A new flexural strength model of CFRP-strengthened RC beams with intermediate crack induced debonding failure. Composite Structures, 308, 116681. doi:10.1016/j.compstruct.2023.116681.

[41] Fayyadh, M. M., & Razak, H. A. (2021). Externally bonded FRP applications in RC structures: A state-of-the-art review. Jordan Journal of Civil Engineering, 15(2), 157–179.

[42] Askar, M. K., Hassan, A. F., & Al-Kamaki, Y. S. S. (2022). Flexural and shear strengthening of reinforced concrete beams using FRP composites: A state of the art. Case Studies in Construction Materials, 17. doi:10.1016/j.cscm.2022.e01189.

[43] Liu, F., Wu, B., & Wei, D. (2009). Failure modes of reinforced concrete beams strengthened with carbon fiber sheet in fire. Fire Safety Journal, 44(7), 941–950. doi:10.1016/j.firesaf.2009.05.006.

[44] Ahmed, A., & Kodur, V. (2011). The experimental behavior of FRP-strengthened RC beams subjected to design fire exposure. Engineering Structures, 33(7), 2201–2211. doi:10.1016/j.engstruct.2011.03.010.

[45] Yu, B., & Kodur, V. K. R. (2014). Fire behavior of concrete T-beams strengthened with near-surface mounted FRP reinforcement. Engineering Structures, 80, 350–361. doi:10.1016/j.engstruct.2014.09.003.

[46] Jiangtao, Y., Yichao, W., Kexu, H., Kequan, Y., & Jianzhuang, X. (2017). The performance of near-surface mounted CFRP strengthened RC beam in fire. Fire Safety Journal, 90, 86–94. doi:10.1016/j.firesaf.2017.04.031.

[47] Truong, G. T., Lee, H. H., & Choi, K. K. (2018). Flexural behavior of RC beams strengthened with NSM GFRP strips after exposed to high temperatures. Engineering Structures, 173, 203–215. doi:10.1016/j.engstruct.2018.06.110.

[48] Nguyen, V. N., & Van Cao, V. (2023). NSM GFRP Strengthening of Reinforced Concrete Beams after Exposure to Fire: Experiments and Theoretical Model. Journal of Composites for Construction, 27(1), 04022086. doi:10.1061/jccof2.cceng-3933.

[49] ASCE/SEI 41-17. (2017). Seismic Evaluation and retrofit of existing Buildings. American Society of Civil Engineers (ASCE), Reston, United States.

[50] Wickström, U. (1986). A very simple method for estimating temperature in fire exposed concrete structures. Fire Technology, Technical Report, Statens Provningsanst, Boras, Sweden.

[51] Purkiss, J. A., & Li, L. Y. (2013). Fire safety engineering design of structures (3rd Ed.). CRC Press Taylor & Francis, Boca Raton, United States. doi:10.1201/b16059.

[52] Eamon, C. D., & Jensen, E. (2012). Reliability analysis of prestressed concrete beams exposed to fire. Engineering Structures, 43, 69–77. doi:10.1016/j.engstruct.2012.05.016.

[53] ACI 318-19. (2019). Building code requirements for structural concrete. American Concrete Institute (ACI), Michigan, United States.